Robotica (1999) volume 17, pp. 59–70. Printed in the United Kingdom © 1999 Cambridge University Press

Dynamic instant gait stability measure for quadruped walking robot

Tae-Wan Koo and Yong-San Yoon

Department of Mechanical Engineering, Korea Advanced Institute of Science and Technology, ME3022, Taejon, 305–701 (Korea).

(Received in Final Form: April 21, 1998)

SUMMARY

A mathematic model is developed for a quadruped walking robot to investigate the dynamic stability considering all the inertial effects in the system including those of legs. The dynamic model is derived based on Lagrange's equation using matrix-vector notations for the simpler expression. Then an instant gait stability measure is proposed to apply to dynamic gait as well as static gait. The gait stability measure is obtained from the angular momentum of the system about the supporting edges in the quadrupedal gait of $+x$ type. The validity of the gait stability measure is examined along with the gait stability analysis for several representative gait parameters using the developed dynamic model.

KEYWORDS: Quadruped walking robot; Dynamic model; Gait stability measure; Angular momentum about a line.

1. INTRODUCTION

The walking robots have been vigorously researched by many researchers for the past three deacdes because of the advantages of the superior moblity in irregular terrain and the less hazardous influences on environment comparing with the wheeled vehicle. There are three major types of locomotion: static, quasi-dynamic and dynamic gaits. The static gait is characterized by such a slow motion that its dynamic effect is negligible during the locomotion while the quasi-dynamic and dynamic gaits are fast and their dynamic effects are significant. In determining motion, the static and quasi-dynamic gaits have convex support areas or polygons and their motions are determiend by kinematics while the dyanamic gait has some periods having no support area (dynamic supporting period with one or two leg support) and its motion is determined by kinetics.[1] It is assumed that our walking robot has no flight phase. If the duty factor of a gait is lowered to have longer dynamic supporting period, the actual trajectory may be far off from the desired one and the robot may overturn. To prevent the robot from such overturning, the stability of the gait should be secured.

For the static gait of quadruped walking robot, several works were published regarding for gait stability indices.[2–4] McGhee and Frank[2] defined the support polygon as the convex hull of the supporting feet and the longitudinal stability margin as the shortest distance between the projected center of mass of the system to the ground surface and the boundaries of the support polygon in the direction of travel. Messuri and Klein[3] proposed the energy stability margin (ESM) considering the minimum energy required to tip the system over the edges in a support polygon. Nagy et al.[4] extended the energy stability margin taking both the swing leg and the terrain compliance into consideration. And Zhang and Song[5] analytically investigated the stability of wave-crab gaits of quadruped using the geometric relationship between the projected mass center and the supporting polygon based on the conventional static stabilty margin.

For the dynamic gaits, few works were published not to mention gait stability.[6–15] To show the physical admissibility of a gait, the concept of zero moment point (ZMP) was introduced by Vukobratovic and Stepanonko.[6] For the quasi-dynamic gait. Yoneda and Hirose[7] utilized the ZMP in planning the trajectory for the dynamic and static fusion gait of a quadruped walking robot. And they recently proposed the tumble stability criterion for a quadruped walking robot utilizing the moment about the line segments formed by two supporting feet.[8] Seo and Yoon[9] proposed the dynamic stability margin of a gait as the smallest magnitude of linear impulse making the gait fail. Adachi et al.[10] suggested a condition for continuing the gait in the two-leg supporting period using the kinetic energy of simplified inverted pendulum model. Miyazaki and Arimoto[11] pioneered the stability of a biped locomotion by using the singular perturbation method. Hurmuzlu and Basdogan[12] developed a quatntiative measure to assess the dynamic stability of human locomoation based on the Floquet theory. Lin and Song[13] defined a dynamic stability margin applicable to the static gait using the resultant moment about the boundaries of the support polygon. For the improvement of dynamic quadruped locomotion, Sano and Furusho[14] utilized the quasi-angular momentum. Kimura et al.[15] conducted an extensive work regarding the dynamic gaits of a quadruped robot.

Lots of dynamic models have been suggested for quadruped walking vehicles and most of them are derived based on Newton-Euler equation or the reduced-order models. Though they may be advantageous from the viewpoints of the computational efficiency and the magnification on some physical behaviors, it is difficult in implementing to the model some gait specific conditions such as foot strike as well as the control schemes for the leg joints. With the reduced order model, it may give incorrect

https://doi.org/10.1017/S0263574799001058 Published online by Cambridge University Press

simulation results by disregarding non-negligible factors in the dynamic system. Hence, in our study, a full dynamic model of a quadruped wlaking robot is developed. The dynamic model is obtained analytically using the relative joint coordinates for numerical efficiency.

Appropriate gait stability measure, however, does not exist yet to check the stability for the dynamic gait at every instant. Hence, in this study, we are going to present a dynamic stability measure which is able to assess both the ability to continue the designed dynamic gait and the possibility of toppling over a support edge by using the angular momentum about the edge at every instant of the walking.

In Section 2, the dynamic model of the quadruped walking robot is derived for the system shown in Figure 1. The robot consists of trunk body and four legs each of which has three actuated joints: two for hip and one for knee. The dynamic model is formulated using Lagrange's equation in vector form. In Section 3, the dynamic stability measure using the angular momentum of the robot system is proposed. And the simulation results and discussions are presented in Section 4.

2. DYNAMIC MODEL OF QUADRUPED WALKING ROBOT

In this section, firstly we apply Lagrange's equation to derive the 18 equations of motion for the whole system which has no constraint from the ground contact of the supporting feet. The derived equation also includes the inertia effects of the legs; one leg mass of our robot model amounts to 15% of the total mass (Table I). We then implement the kinematic constraints due to the ground contact of the feet as a spherical joint and the ground reaction forces are determined analytically. The collision effect of the foot strike is considered in the last part of this section.

2.1 Unconstrained equation of motion

All the bodies in the system are assumed to be rigid and the system has the inertial reference frame {E} and the trunk body fixed reference frame {B} as shown in Figure 1. For convenience, the origin of {B} is set to the center of gravity (CG) of the trunk.

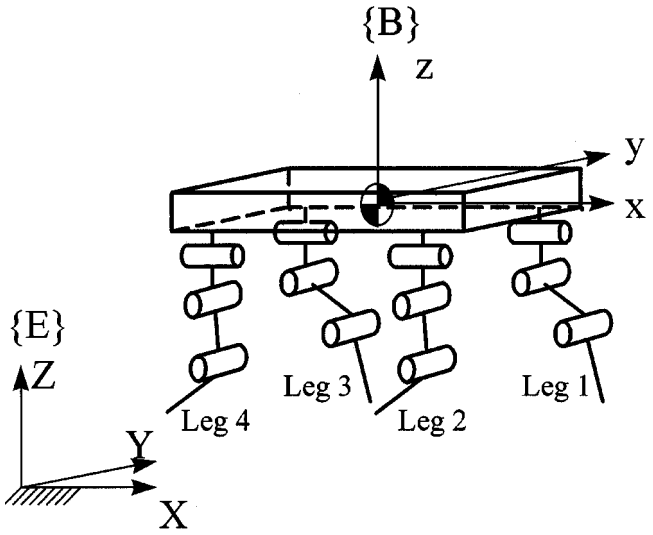

Fig. 1. Schematic diagram for quadruped walking robot

Firstly the generalized coordinate vector $\mathbf{q} \in \mathbf{R}^{18}$ is chosen as the 6 spatial coordinates of the trunk and 12 rotational coordinates of the joint angles as follows:

$$\mathbf{q} = [\mathbf{x}_B^T \ \phi_B^T \ \theta_1^T \ \theta_2^T \ \theta_3^T \ \theta_4^T]^T \tag{1}$$

Here, Bryant angles are used to describe the orientation of the trunk and the relative joint coordinates are used for the joint angles in each leg. The Bryant angles[16] are defined as successive three counterclockwise rotations about x-, y-, and z-axes and are assembled in a vector $\phi_B^T = [\phi_{Bx} \ \phi_{By} \ \phi_{Bz}]$. Time derivatives of the Bryant angles are also known as the roll, pitch and yaw rates, respectively.

The Langrangian L of the system is

$$\begin{aligned} L &= K - P \\ &= \frac{1}{2} m_B \dot{\mathbf{x}}_B{}^T \dot{\mathbf{x}}_B + \frac{1}{2} \omega'_B{}^T \mathbf{I}'_B \omega'_B + \sum_{i=1}^{4} \sum_{j=1}^{3} \\ &\left\{ \frac{1}{2} m_{ij} \left(\dot{\mathbf{x}}_B{}^T \dot{\mathbf{x}}_B + \dot{\mathbf{r}}_{ij}{}^T \dot{\mathbf{r}}_{ij} + 2 \dot{\mathbf{x}}_B{}^T \dot{\mathbf{r}}_{ij} \right) + \frac{1}{2} \omega'^T_{if} \mathbf{I}'_{ij} \omega'_{if} \right\} \\ &- \mathbf{g}^T \left\{ \left(m_B + \sum_{i=1}^{4} \sum_{j=1}^{3} m_{ij} \right) \mathbf{x}_B + \sum_{i=1}^{4} \sum_{j=1}^{3} m_{ij} \mathbf{r}_{ij} \right\} \end{aligned} \tag{2}$$

where K and P are the kinetic and potential energies of the system and m_B, m_{ij}, $\mathbf{I}'_B$, $\mathbf{I}'_{ij}$, ω'_B, and ω'_B are the mass parameters, inertia tensors and angular velocity vectors of the trunk body and the link j of the leg i, respectively. Here the inertia tensor and the angular velocity vector of each link in are evaluated in its local frame. The vector $\mathbf{r}_{ij}$ denotes the position vector of the CG of the link j in the leg i in {E}. The mass, moment of inertia and the kinematic parameters for the walking robot model are listed in Table I. The hip locations with respect to {B} are listed in Table II.

Lagrange's equation of motion in a vector form is

$$\frac{d}{dt} \left(\frac{\partial L}{\partial \dot{\mathbf{q}}} \right)^T - \left(\frac{\partial L}{\partial \mathbf{q}} \right)^T = \mathbf{Q}_{nc} \tag{3}$$

where $\mathbf{Q}_{nc} \in \mathbf{R}^{18}$ is the nonconservative force vector applied to the robot system. Then the equation of motion for the unconstrained system is derived as the following matrix-vector form:

$$\mathbf{M}(\mathbf{q})\ddot{\mathbf{q}} + \mathbf{h}(\mathbf{q}, \dot{\mathbf{q}}) = \mathbf{Q}_{nc} \tag{4}$$

where $\mathbf{M} \in \mathbf{R}^{18 \times 18}$ is the mass matrix, $\mathbf{h} \in \mathbf{R}^{18}$ is the force vector containing velocity-dependent forces and gravitational forces. The detailed terms are symbolically presented in Appendix.

2.2 Implementation of kinematic constraints

In this section, the kinematic constraints due to the foot contact with the ground are implemented to Equation (4)

https://doi.org/10.1017/S0263574799001058 Published online by Cambridge University Press

Table I. Mass, moment of inertia, and kinematic parameters of robot model

	Trunk Body	Link 1	Link 2	Link 3
m (Kg)	20.980	3.188	3.565	1.952
I_x $(Kg\text{-}m^2)$	1.450	0.0215	0.0442	0.0585
I_y $(Kg\text{-}m^2)$	2.725	0.0215	0.0442	0.0585
I_z $(Kg\text{-}m^2)$	3.725	0.0072	0.0127	0.0195
Length (m)		0.080	0.302	0.386
Distance of CG from the upper joint (m)		0.039	0.139	0.193

modeling the foot contact as a spherical joint connection. Then the foot contact of a leg produces three holonomic constraints $\mathbf{\Phi}_i \in \mathbf{R}^3$ as

$$\mathbf{\Phi}_i \equiv \mathbf{x}_B + \mathbf{r}_i^{tip}(\phi_B,\ \theta_i) - \mathbf{x}_i^{tip} = \mathbf{0} \tag{5}$$

where $\mathbf{r}_i^{tip}$ and $\mathbf{x}_i^{tip}$ are the displacement vectors from the origin of {B} and {E} to the foot contact positions of leg i, respectively, both expressed in {E}. Then the total constraint equation with n_s feet ground contacted can be written as follows:

$$\mathbf{\Phi} \equiv [\mathbf{\Phi}_1^T \ \ldots \ \mathbf{\Phi}_{n_s}^T]^T = \mathbf{0} \tag{6}$$

Differentiating Equation (6) twice with respect to time, we can get the acceleration constraint equation as

$$\mathbf{\Phi}_\mathbf{q}\ddot{\mathbf{q}} - \gamma(\mathbf{q},\ \dot{\mathbf{q}}) = \mathbf{0} \tag{7}$$

where $\mathbf{\Phi}_q \in \mathbf{R}^{3n_s \times 18}$ is the Jacobian matrix and $\gamma \in \mathbf{R}^{3n_s}$, is the velocity-dependent acceleration vector containing such as the centripetal and Coriolis accelerations.

Equation (7) is appended to Equation (4) forming the constrained equation of motion by introducing Lagrange multiplier λ as

$$\begin{bmatrix} \mathbf{M} & -\mathbf{\Phi}_\mathbf{q}^T \\ \mathbf{\Phi}_\mathbf{q} & \mathbf{0} \end{bmatrix} \begin{Bmatrix} \ddot{\mathbf{q}} \\ \lambda \end{Bmatrix} = \begin{Bmatrix} \mathbf{Q}_{nc} - \mathbf{h} \\ \gamma \end{Bmatrix} \tag{8}$$

where $\lambda \in \mathbf{R}^{3n_s}$ is Lagrange multiplier vector which is identical to the terrain reaction forces of the supporting feet.

2.3 Terrain reaction forces and generalized nonconservative forces

In this section, the terrain reaction forces and the generalized nonconservative forces are evaluated symbolically.

From Equation (6), the Jacobian matrix $\mathbf{\Phi}_\mathbf{q}$ can be partitioned as follows:

$$\mathbf{\Phi}_\mathbf{q} = \begin{bmatrix} \mathbf{\Phi}_{\mathbf{1q}}^T \ldots \mathbf{\Phi}_{n_s\mathbf{q}}^T \end{bmatrix}^T \tag{9}$$

Table II. Hip locations of the legs in {B}

	Hip locations
Hip 1	(0.287, 0.17, 0)
Hip 2	(0.287, −0.17, 0)
Hip 3	(−0.287, 0.17, 0)
Hip 4	(−0.287, −0.17, 0)

Then Lagrange multiplier vector $\lambda \in \mathbf{R}^{2n_s}$ can also be partitioned as $\lambda = [\lambda_1^T \ldots \lambda_{n_s}^T]^T$ where $\lambda_i \in \mathbf{R}^3$.

The generalized nonconservative force vector $\mathbf{Q}_{nc}$ can be obtained using the principle of virtual work. The generalized nonconservative forces acting on the walking system may be categorized into three kinds: the actuating forces, externally applied forces, and the frictional forces at the joints. In this work, the acutating forces are the joint torques and the external forces may apply to the trunk. However, the frictional forces at the joints are not considered since their effects are negligible.

Let's denote the joint driving torques in leg i as τ_i and the external force and torque at the trunk as $\mathbf{f}_t$ and $\mathbf{T}_t$. Then the virtual work done by the nonconservative force is calculated as

$$\begin{aligned} \delta W_{nc} &= \mathbf{Q}_{nc}^T \delta \mathbf{q} \\ &= \mathbf{f}_t^T \delta \mathbf{x}_B + \mathbf{T}_t^T \delta \phi_B + \sum_{i=1}^{4} \tau_i^T \delta\theta \end{aligned} \tag{10}$$

Thus the generalized nonconservative external force vector $\mathbf{Q}_{nc}$ can be obtained as

$$\mathbf{Q}_{nc} = [\mathbf{f}_t^T\ \mathbf{T}_t^T\ \tau_1^T\ \tau_2^T\ \tau_3^T\ \tau_4^T]^T \tag{11}$$

2.4 Foot strike

The colliding phenomenon occurring when the foot strikes the ground is considered in this section. Without modeling the collision at the foot tip, we found from our walking simulation that the tip of the leg may be placed below the ground surface which is not possible for the rigid ground surface.

Assuming that the ideally plastic impact occurs between the colliding foot and the ground surface instantaneously, the collision can be modeled as the occurrence of instantaneous velocity change.[17] Here the ideally plastic impact means that the tip velocity of the colliding foot is vanished right after the foot strike. Then from Lagrange's impulsive equation for a kinematically constrained system with the assumption of ideally plastic input, a differential-algebraic equation is obtained in the following form:[18]

$$\begin{bmatrix} \mathbf{M} & {}^s\mathbf{\Phi}_\mathbf{q}^T & {}^c\mathbf{\Phi}_\mathbf{q}^T \\ {}^s\mathbf{\Phi}_\mathbf{q} & \mathbf{0} & \mathbf{0} \\ {}^c\mathbf{\Phi}_\mathbf{q} & \mathbf{0} & \mathbf{0} \end{bmatrix} \begin{Bmatrix} \nabla\dot{\mathbf{q}} \\ \lambda^s \\ \lambda^c \end{Bmatrix} = \begin{Bmatrix} \mathbf{0} \\ \mathbf{0} \\ -\mathbf{v}^c \end{Bmatrix} \tag{12}$$

where the vector $\mathbf{v}^c \in \mathbf{R}^{3n_c}$ is the velocities of the n_c colliding

https://doi.org/10.1017/S0263574799001058 Published online by Cambridge University Press

feet, ${}^{s}\mathbf{\Phi}_{\mathbf{q}} \in \mathbf{R}^{3n_s \times 18}$ and ${}^{c}\mathbf{\Phi}_{\mathbf{q}} \in \mathbf{R}^{3n_s \times 18}$ are the Jacobian matrices of the originally contacted feet and the colliding feet, respectively, $\lambda^s \in \mathbf{R}^{3n^c}$ and $\lambda^c \in \mathbf{R}^{3n_c}$ are the impact force vectors of the originally contacted feet and the colliding feet, respectively. The instanteous change of velocity due to the collision of feet is determined as $\dot{\mathbf{q}}^+ = \dot{\mathbf{q}}^- + \Delta\dot{\mathbf{q}}$ where the superscripts $-$ and $+$ represent quantities right before and after the collision, respectively.

3. GAIT STABILITY MEASURE FOR QUADRUPED WALKING ROBOT

Consider first the conventional stability measures.[2–5,14] Most of them take only the geometric consideration in evaluating the stability measure not considering the motion of the robot system and the swing leg to be supported neglecting the kinematic states of the system which strongly relate to the system's stability. Thus their application is confined to the static gaits only. And, here, we are proposing a gait stability measure which can be applied at every instant of the dynamic gait as well as the static gait considering the current kinematic states and the effect of the swing leg to be supported.

3.1 Angular momentum about support edge

Several physical quantities such as kinetic energy, linear and angular velocities, angular momentum and moment about a line could be considered for the gait stability. Among them the angular momentum is a vector quantity containing both inertial and motion parameters simultaneously. Even though the kinetic energy and the moment of the system also possess similar features, the directional information can hardly be extracted from the energy quantity and the moment of the system has difficulty in setting the reference value of the system stability. The angular momentum of the walking robot with respect to a ground point can be denoted as a vector and its component along a support edge represents the rotational tendency of the walking robot about the supporting edge. The details are described in the following.

Firstly the linear momentum $\mathbf{L}$ and the angular momentum $\mathbf{H}_B$ about the CG of the trunk (the origin of {B}) are calculated from the following equations,

$$\mathbf{L} = m_B \dot{\mathbf{x}}_B + \sum_{i=1}^{4} \sum_{j=1}^{3} m_{ij} \dot{\mathbf{x}}_{ij} \tag{13}$$

$$\mathbf{H}_B = \sum_{i=1}^{4} \sum_{j=1}^{3} (\mathbf{r}_{ij} \times m_{ij} \dot{\mathbf{x}}_{ij}) + {}^{E}_{B}\mathbf{R} \left[\mathbf{I}'_B \boldsymbol{\omega}'_B + \sum_{i=1}^{4} \sum_{j=1}^{3} \mathbf{I}'_{ij} \boldsymbol{\omega}'_{ij} \right] \tag{14}$$

where $\dot{\mathbf{x}}_{ij}$ is the time derivative of the position vector from the origin of {E} to the mass center of link j of leg i, and ${}^{E}_{B}\mathbf{R} \in \mathbf{R}^{3\times3}$ is the rotational transformation matrix from {B} to {E}. The linear momentum and the angular momentum of the whole system about the CG of the trunk in Equations (13) and (14) are both expressed in {E} and also obtained from the following relations,

$$\mathbf{L} = \left(\frac{\partial K}{\partial \dot{\mathbf{x}}_B} \right)^T, \quad \mathbf{H}_B = {}^{E}_{B}\mathbf{R} \left(\frac{\partial K}{\partial \boldsymbol{\omega}'_B} \right)^T \tag{15}$$

where K denotes the kinetic energy of the whole system. Based on Equations (13) and (14), an angular momentum vector of the system with respect to a point P on the ground, $\mathbf{H}_P$ can be determined with a relative position vector $\mathbf{r}_{B/P}$ from the point P to the origin of {B} expressed in {E} as follows:

$$\mathbf{H}_P = \mathbf{H}_B + \mathbf{r}_{B/P} \times \mathbf{L} \tag{16}$$

Henceforth the calculating procedure for the angular momentum about the edge formed by two feet in ground contact is as follows: Consider a walking robot with a supporting edge l formed by foot i and foot j both in ground contact as shown in Figure 2. With the point P as a point on the edge l, the angular momentum vector of Equation (16) is projected to the edge l and we can obtain the angular momentum component which can be interpreted as the rotational tendency of the system about the edge as

$$H_l = (\mathbf{H}_B + \mathbf{r}_{B/P} \times \mathbf{L}) \cdot \hat{\mathbf{e}}_l \tag{17}$$

where $\hat{\mathbf{e}}_i$ is the unit vector along the edge with positive direction from foot i to foot j as listed in Table III to make outward rotation. Then the unit vector is simply expressed as

$$\hat{\mathbf{e}}_l = \frac{\mathbf{x}_j^{tip} - \mathbf{x}_i^{tip}}{\left\| \mathbf{x}_j^{tip} - \mathbf{x}_i^{tip} \right\|} \tag{18}$$

where $\mathbf{x}_i^{tip}$ and $\mathbf{x}_j^{tip}$ are the position vectors from the origin of {E} to the feet i and j expressed in {E} respectively.

3.2 Gait stability measure using angular momentum

In this section, a gait stability measure is developed utilizing the angular momentum about the support polygon edges. The support polygon may form a convex polygon or a line in accordance with the number of supporting feet. Firstly, restrict our consideration to symmetric, regular, periodic gaits moving forward on the level surface. Secondly, the swing legs are assumed not to cross the supporting legs so

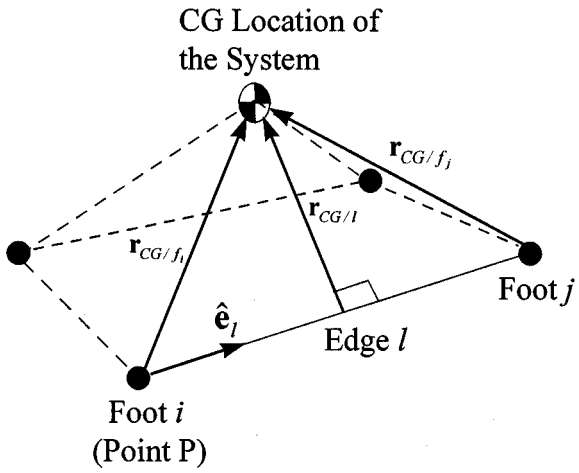

Fig. 2. Supporting edges and CG of the walking robot

https://doi.org/10.1017/S0263574799001058 Published online by Cambridge University Press

Table III. Gait stability values for various supporting edges

Edge Type	Foot ID in an Edge				
	i	j			Stability Measure for an Edge (S_H^l)
Non-diagonal	2	1			$S_H^l = H_l^{ref} - H_l$
	4	2			
	3	4			
	1	3			
Diagonal	4	1	2-leg Support	CG has not passed the edge	$S_H^l = \min(H_l - H_l^{ref}, H_l^{max} - H_l)$
				CG has passed the edge	$S_H^l = H_l^{max} - H_l$
	3	2	3-leg Support	Front Edge	$S_H^l = H_l^{max} - H_1$
				Rear Edge	$S_H^l = H_l^{ref} - H_l$

that forthcoming support polygon be convex. Also we assume that the number of supporting legs is always more than one having duty factor of $0.5 \le \beta < 0.75$.

We define the gait stability measure as the minimal one among the stability values obtained with respect to all the edges in the support polygon at an instant as follows:

$$S_H = min\{S_H^l,\ l = 1, \ldots, n_l\} \tag{19}$$

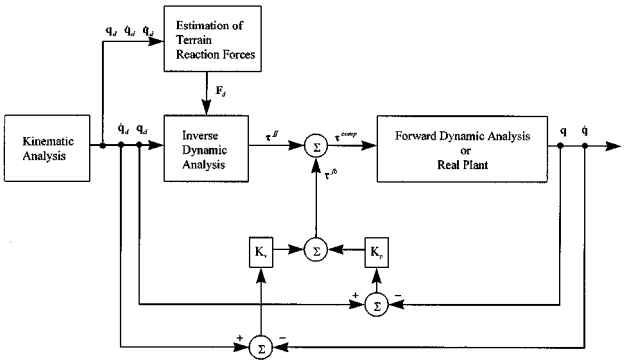

Fig. 3. Block diagram for the feedforward control with PD for quadruped walking robot

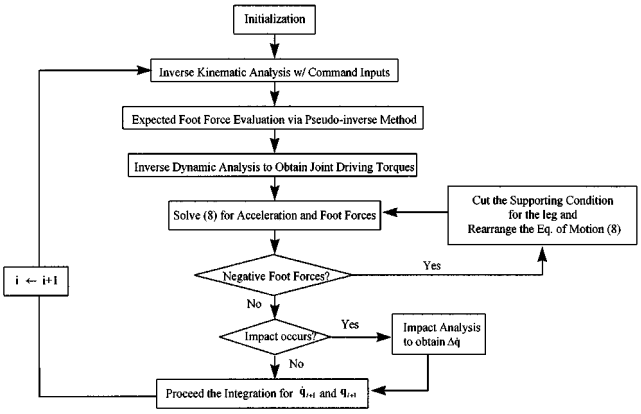

Fig. 4. Flow chart for the simulation of gait dynamics

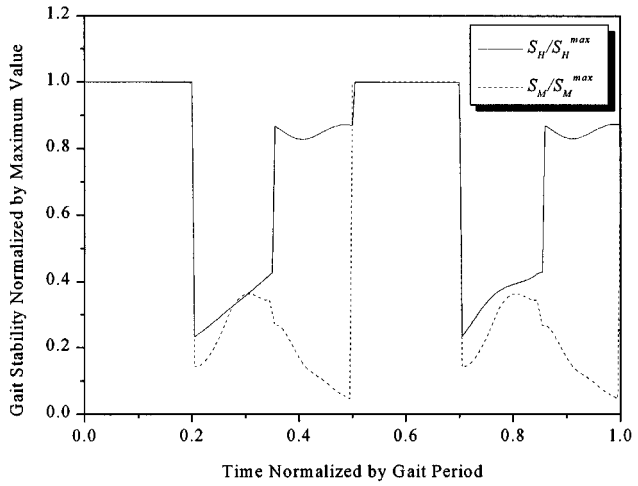

Fig. 5. Comparison of S_m and S_H for the static gait with $\beta = 0.85$, $R = 0.3$m

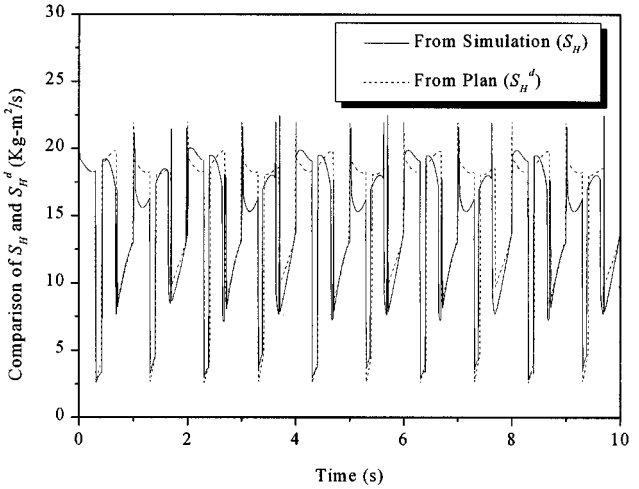

Fig. 6. Results of S_H from gait plan and dynamic simulation for $\beta = 0.65$, $R = 0.3$m and $T = 2$s

https://doi.org/10.1017/S0263574799001058 Published online by Cambridge University Press

where n_l is the number of edges in the support polygon and S_H^l is *the gait stability for the edge l*. To obtain the gait stability for the edge l, firstly the possible edges are classified into two groups: the diagonal edges and the non-diagonal edges. The non-diagonal edge is defined as an edge formed by one of 1–2, 2–4, 3–4 and 1–3 supporting foot pairs where the number indicates the leg identification in Figure 1. The diagonal edge is the one formed by either 1–4 or 2–3 supporting foot pairs. The gait stability value for the non-diagonal edges is considered first in section 3.2.1, and the one for the diagonal edges is considered later in section 3.2.2.

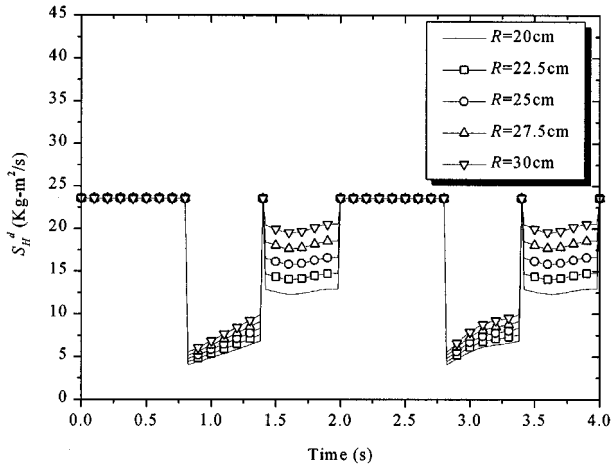

(a) β=0.85, T=4s

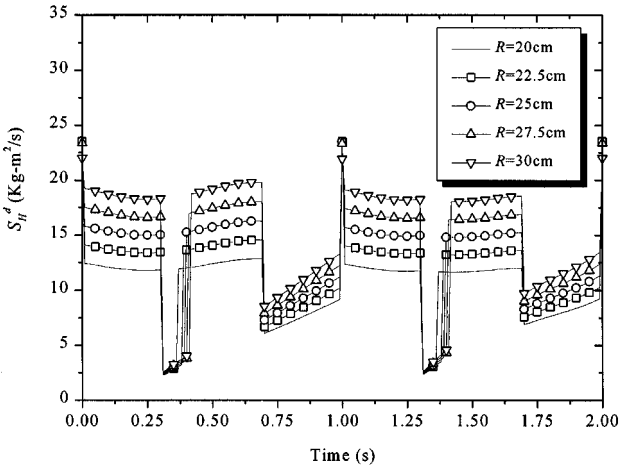

(b) β=0.65, T=2s

Fig. 7. Comparison of planned S_H for various values of foot stroke R

3.2.1 Stability for non-diagonal edges. For the non-diagonal edges, the robot should not be tipped over with respect to any of the edges since there is no other leg available to stabilize the system. Thus the stability values for these edges are defined as

$$S_H^l = H_l^{ref} - H_l \tag{20}$$

Here *the reference angular momentum about an edge l*, H_l^{ref} is defined as the minimum angular momentum to tip over the edge assuming the whole system as a simple inverted pendulum. The CG point of the system is determined as follows:

$$\mathbf{x}_{CG} = \frac{m_B \mathbf{x}_B + \sum_{i=1}^{4}\sum_{j=1}^{3} m_{ij}\mathbf{x}_{ij}}{m_B + \sum_{i=1}^{4}\sum_{j=1}^{3} m_{ij}} \tag{21}$$

Now referring to Figure 2, the potential energy of the system is calculated as $m_{total}\mathbf{g}^T\mathbf{x}_{CG}$ where the total mass of the system, m_{total} is equal to the denominator in Equation (21) and $\mathbf{g}$ is the gravitational acceleration vector. The maximum CG height is equal to $\|\mathbf{r}_{CG/l}\| \cos \psi_l$ where ψ_l is the angle between the edge l and the ground surface. For level walking on a flat surface $\mathbf{g}=[0\ 0\ g]^T$ and $\psi_l=0$. The vector $\mathbf{r}_{CG/l}$ which is orthogonal to the edge l is calculated as follows:

$$\mathbf{r}_{CG/l} = \mathbf{r}_{CG/f_i} - (\mathbf{r}_{CG/f_i}\cdot\hat{\mathbf{e}}_l)\hat{\mathbf{e}}_l \tag{22}$$

where the vector $\mathbf{r}_{a/b}$ denotes the position vector from the point b to the point a expressed in {E}. Then the maximum attainable potential energy of the system about the edge l is $m_{total}g\|\mathbf{r}_{CG/l}\| \cos \psi_l$.

Here, the energy stability margin by Messuri and Klein[3] is determined as $m_{total}(g\|\mathbf{r}_{CG/l}\| \cos \psi_l - \mathbf{g}^T\mathbf{x}_{CG})$ for the edge l. This value is used to determine the magnitude of *the*

Table IV. Overall gait stability for various foot stroke R

R (cm)		20	22.5	25	27.5	30
β=0.85	$min\{S_H^d\}$	3.93	4.27	4.62	4.97	5.33
	$\int_0^T S_H^d dt$	59.6	62.4	65.3	68.2	71.3
β=0.65	$min\{S_H^d\}$	2.14	2.20	2.27	2.33	2.40
	$\int_0^T S_H^d dt$	20.3	22.6	24.9	27.2	29.4

https://doi.org/10.1017/S0263574799001058 Published online by Cambridge University Press

reference velocity vector $\mathbf{v}_{ref}$ by using the concept of energy conservation as follows:

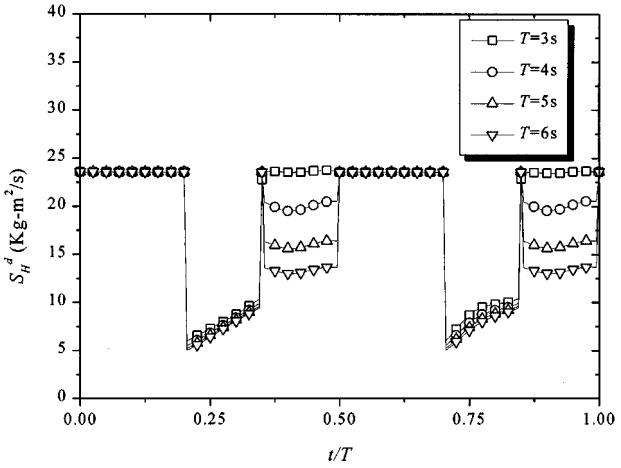

(a) β=0.85, R=30cm

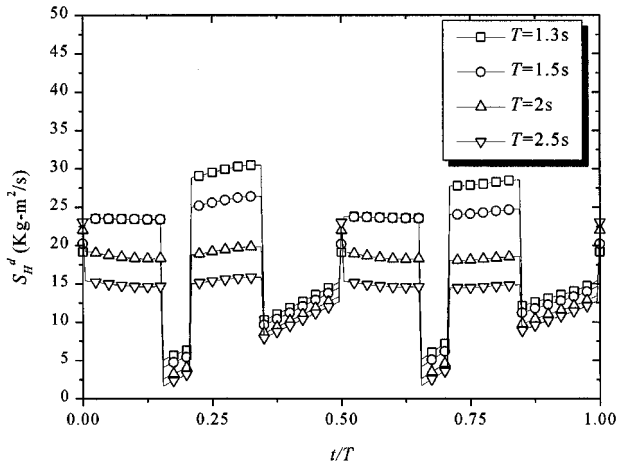

(b) β=0.65, R=30cm

Fig. 8. Comparison of planned S_H for various values of gait period T

$$m_{total}(g\|\mathbf{r}_{CG/l}\|\cos\psi_l - \mathbf{g}^T\mathbf{x}_{CG}) = -\frac{1}{2}m_{total}v_{ref}^2 \tag{23}$$

Then we can compute the magnitude of the reference velocity as $v_{ref}=\sqrt{2(g\|\mathbf{r}_{CG/l}\|\cos\psi_l - \mathbf{g}^T\mathbf{x}_{CG})}$ whose direction is outer normal to the plane formed by the locations of foot, *i*, *j* and the CG point of the system. Thus we obtain the reference veloicty vector $\mathbf{v}_{ref}$ as

$$v_{ref}=\left[\sqrt{2(g\|\mathbf{r}_{CG/l}\|\cos\psi_l - \mathbf{g}^T\mathbf{x}_{CG})}\right]\hat{\mathbf{e}}_{ref} \tag{24}$$

where the unit vector $\hat{\mathbf{e}}_{ref}$ is the direction of the reference velocity defined as

$$\hat{\mathbf{e}}_{ref}=\begin{cases}\dfrac{\mathbf{r}_{CG/f_i}\times\mathbf{r}_{CG/f_j}}{\|\mathbf{r}_{CG/f_i}\times\mathbf{r}_{CG/f_j}\|} & \text{if z-component of } \mathbf{r}_{CG/f_i}\times\mathbf{r}_{CG/f_j} \text{ is positive}\\ -\dfrac{\mathbf{r}_{CG/f_i}\times\mathbf{r}_{CG/f_j}}{\|\mathbf{r}_{CG/f_i}\times\mathbf{r}_{CG/f_j}\|} & \text{if z-component of } \mathbf{r}_{CG/f_i}\times\mathbf{r}_{CG/f_j} \text{ is negative}\end{cases} \tag{25}$$

The statements in the right hand side of Equation (25) designate whether the CG point has passed over the edge or not; if the z-component of $\mathbf{r}_{CG/f_i}\times\mathbf{r}_{CG/f_j}$ is positive, CG point has not tipped over the edge yet. Using Equations (22) and (24), the reference angular momentum about edge *l* is computed as follows:

$$H_l^{ref}=(\mathbf{r}_{CG/l}\times m_{total}\mathbf{v}_{ref})\cdot\hat{\mathbf{e}}_l \tag{26}$$

It is worth noting that the stability measure for the edge *l*, S_H^l is positive in the following two cases:

Case 1: The CG point of the whole system has not passed over the edge and H_l is smaller than H_l^{ref} so that the system may not topple over the edge.

Case 2: The CG point of the whole system has passed over the edge but the system is progressing in the stable direction.

For Case 2, H_l^{ref} and H_l have both negative values with H_l having the larger absolute value than H_l^{ref}. Thus the system may not be turned over. Except these two circumstances S_H^l

Table V. Overall stability measure for various gait period T

	$T(s)$	3	4	5	6
β=0.85	$min\{S_H^d\}$	5.81	5.33	5.04	4.85
	$\int_0^T\left(S_H^d/T\right)dt$	19.04	17.81	16.52	15.66
	$T(s)$	1.3	1.5	2	2.5
β=0.65	$min\{S_H^d\}$	4.85	3.92	2.40	1.49
	$\int_0^T\left(S_H^d/T\right)dt$	19.96	18.54	14.73	12.24

https://doi.org/10.1017/S0263574799001058 Published online by Cambridge University Press

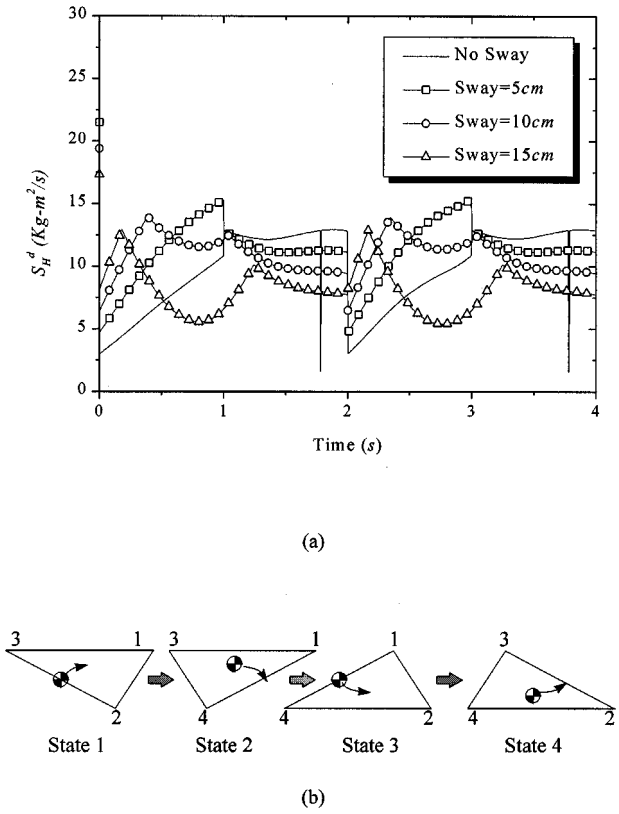

Fig. 9. Planned gait stability (S_H^d) for various amplitude of sway and initial states of each support polygon for $\beta = 0.75$

is negative meaning that the system is in a dynamically unstable state.

3.2.2. Stability for diagonal edges. Now consider the stability value for the diagonal edge formed by either 1–4 or 2–3 supporting. The diagonal edges occur when the supporting legs are less than four and there are at least one swing leg which may stabilize the robot motion. Then the following four cases may describe all the possible occurrences in evaluating the stability value for a diagonal edge:

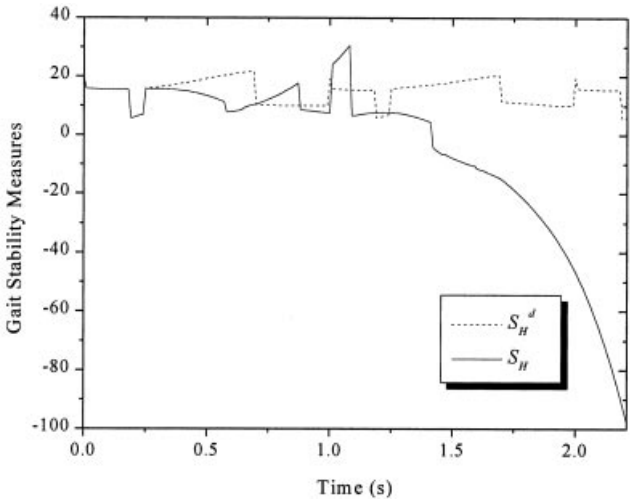

Fig. 10. Overturning of the robot sway motion of 5 *cm* is given ($\beta = 0.65$)

Case 1: Two-leg supporting period and the CG of the system has not passed over the diagonal edge yet.

Case 2: Two-leg supporting period and the CG of the system has passed over the diagonal edge.

Case 3: Three-leg supporting period and the diagonal edge is in the front side of the support polygon.

Case 4: Three-leg supporting period and the diagonal edge is in the rear side of the support polygon.

For Case 1, we introduce *the maximum angular momentum* H_l^{max} about the diagonal edge as the angular momentum about the edge l when the CG of the system is to move at the maximum velocity of swing leg's tip as follows:

$$H_l^{max} = (\mathbf{r}_{CG/l} \times m_{total} \mathbf{v}_{tip}^{max}) \cdot \hat{\mathbf{e}}_l \qquad (27)$$

where $\mathbf{v}_{tip}^{max}$ is the maximum velocity vector of the swing

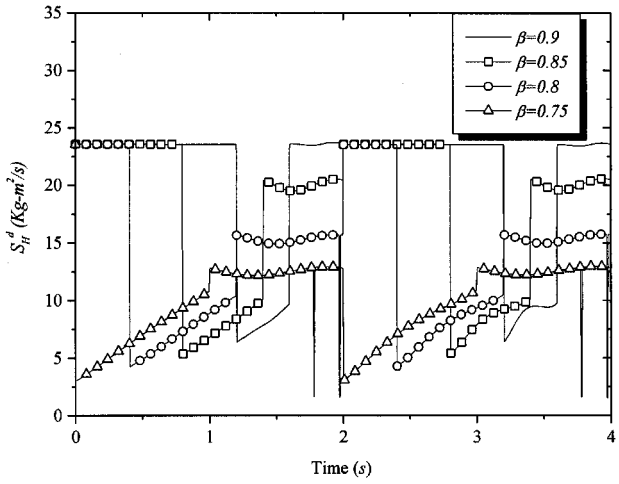

(a) Static gaits (R=30*cm*, T=4*s*)

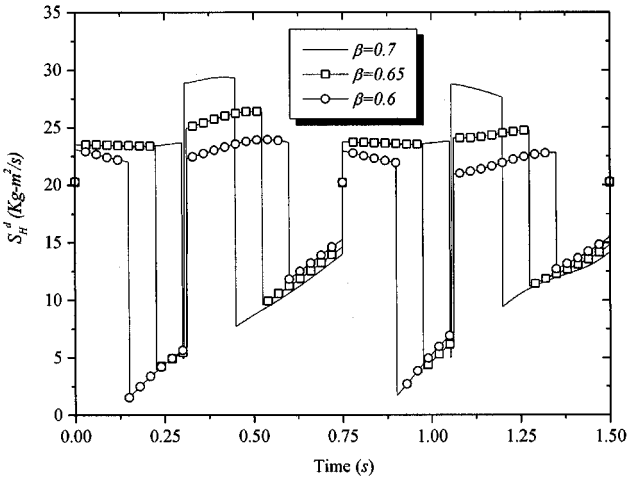

(b) Dynamic gaits (R=30*cm*, T=1.5*s*)

Fig. 11. Comparison of planned S_H for various values of duty factor β

https://doi.org/10.1017/S0263574799001058 Published online by Cambridge University Press

Table VI. Overall stability measure for various duty factor β

	β	0.9	0.85	0.8	0.75
Static & quasi-dynamic Gaits (T=4s)	$min\{S_H^d\}$	6.37	5.33	4.25	1.57
	$\int_0^T \left(S_H^d/T\right)dt$	82.14	71.26	55.32	39.28
	β	0.7	0.65	0.6	
Dynamic Gaits (T=2s)	$min\{S_H^d\}$	4.91	3.92	1.53	
	$\int_0^T \left(S_H^d/T\right)dt$	29.24	27.80	25.27	

leg's tip.

Then the stability value about the diagonal edge is

$$S_H^l = \min\left(H_l - H_l^{ref},\ H_l^{max} - H_l\right) \tag{28}$$

By a heuristic judgment, we may say that the gait fails when the CG of the walking robot advances faster than the swing leg. Note that the first term in the parenthesis of (28) implies the capability of passing over the diagonal edge and the second term gives the excessiveness of the system's momentum compared with the swing leg speed.

For Case 2, we define the stability value as

$$S_H^l = H_l^{max} - H_l \tag{29}$$

In this circumstance, the system is just waiting for the foot of swing leg to reach the ground and the CG of the system should not move faster than the swing leg so as not to stumble.

For Case 3 there is a swing leg in the front of the diagonal edge. To prevent the system from stumbling over the landing foot, it is desired that the tip of swing leg steps forward sufficiently faster than the advance of CG of the system. Thus the stability measure in this case is defined similarly to Case 2 as

$$S_H^l = H_l^{max} - H_l \tag{30}$$

For Case 4, it is desired that the CG of the system should not be turned over the rear diagonal edge in the gait moving forward. Thus the stability value for this circumstance can be defined as follows:

$$S_H^l = H_l^{ref} - H_l \tag{31}$$

In Equations (28) through (31), procedures for evaluating H_l^{ref} and H_l for a diagonal edge l is identical to those for the case of the non-diagonal edges.

Now we have formulated the stability values based on angular momentum about all the possible edges for the quadrupedal gait. The stability values for all the possible edges are summarized in Table III. The stability values for all the supporting edges at an instant calculated from Euqations (20), (28), (29), (30) and (31) are substituted into the right-hand-side of Equation (19) and the gait stability measure at the instant is calculated.

It is worth noting that for the wave-crab gaits the front direction is determined from the crab angle[5] α and the term *front* and *rear* we used above can also be designated in accordance with the crab angle. Thus the gait stability measure for the wave-crab gait can also be obtained. The crab angle is defined to be the angle from the longitudinal body axis to the crab axis (the moving direction of the wave-crab gait) measured in counterclockwise direction.

Also it should be noted that the proposed stability measure and the energy stability margin (ESM) by Messuri and Klein[3] commonly uses the maximum attainable potential energy which comes from a simple inverted pendulum model by ignoring the variation of the joint angles of the legs, but the proposed one differs from the ESM in utilizing this static quantity to evaluate the stability value for each supporting edge considering that the proposed one uses this static quantity to obtain the reference velocity vector for an edge from Equation (24) by using the concept of energy conservation, which is used to evaluate the reference angular momentum about the edge l, H_l^{ref} as shown in Equation (26). Then this value is subtracted by the angular momentum about edge l H_l, to find the stability value as Equation (20). Here, H_l contains the motion parameters such as joint angle variations seeing that H_l is defined as Equation (17). Thus, the proposed measure also takes kinematic states of the system into consideration. In contrast, the ESM considers the maximum attainable potential energy itself to be the stability value about an edge being considered without including the kinematic states of the system. And the measure suggested by Nagy et al.[4] considers the swing leg's position neglecting the kinematic states of the system into acocunt.

For the tumble stability criterion by Yoneda and Hirose,[8] since they utilized the moment of the robot system about only the non-diagonal edges defined in Section 3.2, the tumble stability margin does not give the gait stability during the two leg support phase with diagonal edges. But the tumble stability margin may be stated as a dynamic stability measure since it gives the stability measure for the case of two leg support phases with non-diagonal edges, which the conventional static stability margin does not. And the dynamic stability measure proposed here gives the gait stability value at every instant of any circumstances the walking robot may confront.

https://doi.org/10.1017/S0263574799001058 Published online by Cambridge University Press

4. RESULTS AND DISCUSSIONS

In this section, gait stability analyses are performed to show the validity of the proposed gait stability measure for both dynamic and static gaits. Also the relationship between the gait stability measure and several gait parameters is investigated. In this study, the $+x$ type gait from the gait classification by McGhee and Frank[2] is mainly taken into consideration for demonstrating the results since the gaits of the $+x$ type are adequate for attaining the forward walking gaits including the dynamic gaits of trot type by tuning several gait parameters. The $+x$ gait is characterized by its leg swing sequence and the sequence is one of 4–2–3–1, 2–3–1–4, 3-1-4-2, and 1–4–2–3.

4.1 Simulation results for the static and dynamic gaits

For the static gaits, the kinematic and inverse dynamic analyses may suffice for observing the gait stability with the CG of the system lying within the support polygon. For the dynamic gaits, however, it is required to perform the dynamic analysis to check the gait stability.

In dynamic simulations, the feedforward control with PD which is a family of the computed torque control is adopted to control the leg joints since the control scheme shows better control performance requiring the smaller joint torques than the simple PID control without feedforward term. Block diagram of the control scheme for a quadruped walking robot is presented in Figure 3. The position gain parameter k_p is chosen to be an adequate value keeping the system stable as well as giving small errors in joint angles and the velocity gain parameter k_v is chosen to have critical damping feature; $k_p = 700$ and $k_v = 2\sqrt{k_p}$. The pseudo-inverse method is adopted for estimating the terrain reaction forces which is required for the feedforward joint torque values. The result from the pseudo-inverse method agrees well with the foot forces from Equation (8). The overall procedure for gait dynamic simulation is shown in Figure 4.

Figure 5 shows the comparison of the conventional gait stability margin S_M and the proposed stability measure S_H for one period of static wave gait having the duty factor $\beta = 0.85$, the foot stroke $R = 0.3m$ and the gait period $T = 4s$ without sway motion of the turnk. The sequence of the leg swing for this static gait is 4–2–3–1. The gait velocity V_g is obtained from the relation

$$V_g = \frac{R}{\beta T} \tag{32}$$

The conventional stability margin is defined on the ground as the shortest distance between the vertical projection of CG and the boundaries of the support polygon.[5] Here the center of pressure, instead of the CG of the system, is used in evaluating S_M since the center of pressure expresses the dynamic state of walking robot better than the center of gravity of the system. In Figure 5 both S_M and S_H are plotted after normalized by their maximum values. It is seen that S_M and S_H have similar patterns over a gait period but S_H has mostly higher values in three leg supporting phases having the front diagonal edge. This feature results from taking the swing leg into consideration, that is, there is a swing leg in front of the diagonal edge as stated earlier for Case 3 in Section 3.2.2. Here we suppose that an edge is defined to be *active* when the stability value for the edge is smallest among the stability values for all the edges in a support polygon at an instant. In case of three leg supporting phases having the front diagonal edge, the stability value about the diagonal edge becomes active, thus the stability value about the diagonal edge from Equation (30) becomes the gait stability measure for this circumstance according to Equation (19). In Equation (30), the stability value for a diagonal edge is defined to be the subtraction of the angular momentum of the system from the maximum angular momentum since the system's angular momentum should not be too excessive so as not for the system to proceed its movement before the forthcoming support leg, which is the swing leg at the moment, reaches the place at whch the swing leg will contact the surface ground.

It should be noted that the primary difference between the proposed stability measure and the conventional static stability measure comes from whether the motion of the robot system is taken into consideration or not. We defined the dynamic stability measure considering the robot's motion based on the angular momentum which the robot system possesses at an instant, but the conventional static stability margin is defined geometrically considering the distance between each support edge and the projected mass center. And it should be noted that the similar feature between S_M and S_H results from that the active edge is identical to each other at every instant over the entire period of this static gait.

In Figure 6, the gait stability measures for the planned gait (S_H^d) and the dynamic simulation (S_H) over the five gait periods are shown for the dynamic wave gait of $\beta = 0.65$, $R = 0.3m$, and $T = 2s$ with 1–4–2–3 leg swing sequence without sway motion. The simulated result shows the periodic feature and mostly follows the planned one and it is worth noting that the gait stability is not able to be assessed for the gaits having $\beta < 0.75$ with the conventional static stability margin since there are some phases having the dynamic support (two leg support).

4.2 Relationship between gait parameters and gait stability measure

Several alternatives are possible for describing the overall gait stability measure for a given gait. In this study the minimum value and the integrated value of the stability measure for one gait period are chosen as the possible candidates of the overall gait stability measure.

McGhee and Frank shows in their work that the longitudinal stability margin s is[2]

$$s = \left(1 - \frac{3}{4\beta}\right) R \tag{33}$$

Equation (33) states that the gait stability increases accordingly with the larger foot stroke and duty factor. Kimura et al. demonstrated with their theory and the walking experiments that the shorter a gait period is, the more stable the quadruped is in the dynamic gait.[15]

Figure 7 shows the gait staiblity measure over one gait

https://doi.org/10.1017/S0263574799001058 Published online by Cambridge University Press

period for the various foot stroke *R*. For the static gaits, the overall gait stability measures increase accordingly with the larger foot stroke values, which agrees with McGhee and Frank's work. For the dynamic gaits, there are similar charactreristics to the static ones but differences of the overall gait stability measures for varying the foot stroke are not as much as for the static gaits (Table IV). Figure 8 shows the relationship between the gait stability measure and the gait period *T*. It is observed that shorter gait period increases the gait stability measure both in static and dynamic gaits (Table V) consistently with the result of Kimura et al. The feature can be explained from the fact that faster gait velocity of Equation (32) from shorter gait period makes the swing leg's foot move faster so that the gait stability measure for the front diagonal edge in Equation (30) may become larger. This kind of improvement in gait stability can be achieved by enlarging the foot strike time margin suggested by Seo and Yoon.[9]

The gait stability measure also can be varied when the sway motion of the turnk body is considered. In this study, the sway motion is modeled as a simple sinusoidal trajectory of trunk motion in the lateral direction. Figure 9a shows the results with $\beta = 0.75$. Increasing the sway amplitude changes the gait stability measure but not in a monotonic way. This results from the fact that the stability value for each edge formed by 1–3 or 2–4 footing becomes small while increasing the sway amplitude (Figure 9b). For dynamic gaits with intentional sway motion, it is shown that the robot may be out of its regular step since an excessive sway motion induces large lateral oscillation resulting in overturning as shown in Figure 10. It is worth noting that even though no sway motion is intended at the planning stage of the dynamic gaits of $\beta < 0.75$, the system suffers the same sway motion during the dynamic support period. Thus the intentional sway motion in the planning of the dynamic gaits may not improve the gait stability easily as in the case of static gaits.

It is commonly known that the gait stability increases as the duty factor gets larger. This fact can also be shown in Figure 11 and Table VI, for both the static and dynamic gaits. The gait period of the dynamic gait is lowered to 1.5 seconds since the higher gait period makes the gait less stable. The lower peak which emerges when $\beta = 0.75$ is due to the undesired two-leg supporting period of Case 1in Section 3.2.2.

5. CONCLUSIONS

In this study, a dynamic model of quadruped walking robot have been derived mathematically using Lagrange's equation. Then a gait stability measure is proposed based on the angular momentums about all the edges in a support polygon to assess the stability of the dynamic gaits as well as the static gaits at each instant. The gait stability of the dynamic and static gaits of $+x$ type is investigated successfully varying several representative gait parameters. The proposed gait stability measure can be utilized in designing the optimal trajectory of the quadrupedal walking gaits and also be extended to other multi-legged walking robots such as haxapod walking robots.

References

1. H.-J. Hong and Y.-S. Yoon, "Numerical Simulation of Dynamic Gait of Quadruped Walking Robot" *SME Trans. Robotics Research* **2**(2), 11–36 (1992).
2. R.B. McGhee and A.A. Frank, "On the Stability Properties of Quadruped Creeping Gaits" *Mathematical Biosciences* **3**, 331–351 (1968).
3. D.A. Messuri and C.A. Klein, "Automatic Body Regulation for Maintaining Stability of a Legged Vehicle during Rough Terrain Locomotion" *IEEE J. Robotics and Automation* **RA-1**(3), 132–141 (1985).
4. P.V. Nagy, S. Desa and W.L. Whittaker, "Energy-Based Stability Measures for Reliable Locomotion of Statically Stable Walkers: Theory and Application" *Int. J. Robotics Research* **13**(3), 272–287 (1994).
5. C.-D. Zhang and S.-M. Song, "Stability Analysis of Wave-Crab Gaits of a Quadruped" *J. Robotic Systems* **7**(2), 243–276 (1990).
6. M. Vukobratovic and J. Stepanko, "Mathematical Models of General Anthropomorphic Systems" *Mathematical Biosciences* **17**, 191–242 (1973).
7. K. Yoneda and S. Hirose, "Dynamic and Static Fusion Gait of a Quadruped Walking Vehicle on a Winding Path" *Advanced Robotics* **9**(2), 125–136 (1995).
8. K. Yoneda and S. Hirose, "Tumble Stability Criterion of Integrated Locomotion and Manipulation" *Proc. IROS 96* (1996) pp. 870–876.
9. Y.-J. Seo and Y.-S. Yoon, "Design of a Robust Dynamic Gait of the Biped using the Concept of Dynamic Stability Margin" *Robotica* **13**, Part 5, 461–468 (1995).
10. H. Adachi, N. Koyachi and E. Nakano, "Mechanism and Control of a Quadruped Walking Robot" *IEEE Control System Mag.* **8**(5), 14–19 (1988).
11. F. Miyazaki and S. Arimoto, "A Control Theoretic Study on Dynamical Biped Locomation" *ASME J. Dynamic Systems, Measurement and Control* **102**, 233–239 (1980).
12. Y. Hurmuzlu and C. Basdogan, "On the Measurement of Dynamic Stability of Human Locomotion" *ASME J. Biomechanical Eng.* **116**, 30–36 (1994).
13. B.S. Lin and S.-M. Song, "Dynamic Modeling, Stability and Energy Efficiency of a Quadrupedal Walking Machine" *IEEE Int. Conf. on Robotics and Automation* (1993) pp. 367–373.
14. A. Sano and J. Furusho, "Evaluation of a Reduced Order Model for Quadruped System and Proposition of a Walking Control Method Using Quasi-Angular Momentum" *J. Robotics and Mechatronics* **5**(6), 582–584 (1993).
15. H. Kimura, I. Shimoyama and H. Miura, "Dynamics in the Dynamic Walk of a Quadruped Robot" *Advanced Robotics* **4**(3), 283–301 (1990).
16. P.E. Nikravesh *Computer-Aided Analysis of Mechanical Systems* (Prentice-Hall, 1988).
17. J. Wittenburg, *Dynamics of Systems of Rigid Bodies* (Teubner, Stuttgart, 1977).
18. E.J. Haug, S.-C. Wu, and S.-M. Yang, "Dynamics of Mechnical Systems with Coulomb Friction, Stiction, Impact and Constraint Addition-Deletion — I *Mechanism and Machine Theory* **21**(5), 401–406 (1986).

APPENDIX DETAILED TERMS IN THE DYNAMIC MODEL

The 18×18 mass matrix **M** and the 18×1 vector **h** in Equation (4) are

https://doi.org/10.1017/S0263574799001058 Published online by Cambridge University Press

$$\mathbf{M(q)}=\begin{bmatrix} \left(m_B+\sum_{i,j} m_{ij}\right)\mathbf{I}_{3\times 3} & \sum_{i,j}\mathbf{K}^*_{ij} & \sum_{j=1}^{3}\mathbf{L}^*_{1j} & \sum_{j=1}^{3}\mathbf{L}^*_{2j} & \sum_{j=1}^{3}\mathbf{L}^*_{3j} & \sum_{j=1}^{3}\mathbf{L}^*_{4j} \\ & \mathbf{I}^*_{\phi} & \sum_{j=1}^{3}\mathbf{P}^*_{1j} & \sum_{j=1}^{3}\mathbf{P}^*_{2j} & \sum_{j=1}^{3}\mathbf{P}^*_{3j} & \sum_{j=1}^{3}\mathbf{P}^*_{4j} \\ & & \sum_{j=1}^{3}\mathbf{I}^*_{1j} & \mathbf{0} & \mathbf{0} & \mathbf{0} \\ & & & \sum_{j=1}^{3}\mathbf{I}^*_{2j} & \mathbf{0} & \mathbf{0} \\ & (Sym.) & & & \sum_{j=1}^{3}\mathbf{I}^*_{3j} & \mathbf{0} \\ & & & & & \sum_{j=1}^{3}\mathbf{I}^*_{4j} \end{bmatrix}$$

$$\mathbf{h(q,\dot{q})}=[\mathbf{h}_x^T\ \mathbf{h}_\phi^T\ \mathbf{h}_{\phi_1}^T\ \mathbf{h}_{\phi_2}^T\ \mathbf{h}_{\phi_3}^T\ \mathbf{h}_{\phi_4}^T]^T \tag{A1}$$

All the coefficient matrices in (A1) are $\mathbf{R}^{3\times 3}$ defined as

$$\mathbf{I}^*_\phi=\mathbf{A}_\phi{}^T\mathbf{I}'_B\mathbf{A}_\phi+\sum_{i=1}^{4}\sum_{j=1}^{3}\left(-m_{ij}\mathbf{A}_\phi{}^T\tilde{\mathbf{s}}_{ij}\tilde{\mathbf{s}}_{ij}\mathbf{A}_\phi+\mathbf{Q}_{ij}{}^T\mathbf{I}'_{ij}\mathbf{Q}_{ij}\right)$$

$$\mathbf{I}^*_{ij}=m_{ij}\mathbf{J}_{ij}{}^T\mathbf{J}_{ij}+\mathbf{R}_{ij}{}^T\mathbf{I}'_{ij}\mathbf{R}_{ij}$$
$$\mathbf{K}^*_{ij}=-m_{ij}{}^E_B\mathbf{R}\tilde{\mathbf{s}}_{ij}\mathbf{A}_\phi$$
$$\mathbf{L}^*_{ij}=m_{ij}{}^E_B\mathbf{R}\mathbf{J}_{ij}$$
$$\mathbf{P}^*_{ij}=m_{ij}\mathbf{A}_\phi{}^T\tilde{\mathbf{s}}_{ij}\mathbf{J}_{ij}+\mathbf{Q}_{ij}{}^T\mathbf{I}'_{ij}\mathbf{R}_{ij} \tag{A2}$$

The superscript * is used to denote the corresponding matrices to the mass matrices.

The vectors in (A1) are all in $\mathbf{R}^3$ defined as

$$\mathbf{h}_x=\left[\sum_{i=1}^{4}\sum_{j=1}^{3}\dot{\mathbf{K}}^*_{ij}\right]\dot{\boldsymbol{\phi}}_B+\sum_{i=1}^{4}\left[\sum_{j=1}^{3}\dot{\mathbf{L}}^*_{ij}\right]\dot{\boldsymbol{\theta}}_i+m_{total}\mathbf{g}$$

$$\mathbf{h}_\phi=\dot{\mathbf{I}}^*_\phi\dot{\boldsymbol{\phi}}_B-\frac{1}{2}\dot{\boldsymbol{\phi}}_B{}^T\frac{\partial\mathbf{I}^*_\phi}{\partial\boldsymbol{\phi}_B}\dot{\boldsymbol{\phi}}_B$$
$$+\sum_{i=1}^{4}\sum_{j=1}^{3}\left[\dot{\mathbf{K}}^{*T}_{ij}\dot{\mathbf{x}}_B-\dot{\mathbf{x}}_B{}^T\frac{\partial\mathbf{K}^*_{ij}}{\partial\boldsymbol{\phi}_B}\dot{\boldsymbol{\phi}}_B+\dot{\mathbf{P}}^*_{ij}\dot{\boldsymbol{\theta}}_i\right.$$
$$\left.-\dot{\mathbf{x}}_B{}^T\frac{\partial\mathbf{L}^*_{ij}}{\partial\boldsymbol{\phi}_B}\dot{\boldsymbol{\theta}}_i-\dot{\boldsymbol{\phi}}_B{}^T\frac{\partial\mathbf{P}^*_{ij}}{\partial\boldsymbol{\phi}_B}\dot{\boldsymbol{\theta}}_i+m_{ij}\mathbf{g}^T\frac{\partial{}^E_B\mathbf{R}}{\partial\boldsymbol{\phi}_B}\mathbf{s}_{ij}\right.$$

$$\mathbf{h}_{\theta_i}=-\frac{1}{2}\boldsymbol{\phi}_B^T\frac{\partial\mathbf{I}^*_\phi}{\partial\boldsymbol{\theta}_i}\boldsymbol{\phi}_B+\sum_{j=1}^{3}\left[\dot{\mathbf{L}}^{*T}_{ij}\dot{\mathbf{x}}_B+\dot{\mathbf{P}}^{*T}_{ij}\boldsymbol{\phi}_B+\dot{\mathbf{I}}^*_{ij}\boldsymbol{\theta}_i\right.$$
$$-\sum_{j=1}^{3}\left[\frac{1}{2}\dot{\boldsymbol{\theta}}_i{}^T\frac{\partial\mathbf{I}^*_{ij}}{\partial\boldsymbol{\theta}_i}\dot{\boldsymbol{\theta}}_i+\dot{\mathbf{x}}_B{}^T\frac{\partial\mathbf{K}^*_{ij}}{\partial\boldsymbol{\theta}_i}\boldsymbol{\phi}_B+\dot{\mathbf{x}}_B{}^T\frac{\partial\mathbf{L}^*_{ij}}{\partial\boldsymbol{\theta}_i}\dot{\boldsymbol{\theta}}_i\right.$$
$$\left.+\dot{\boldsymbol{\phi}}_B{}^T\frac{\partial\mathbf{P}^*_{ij}}{\partial\boldsymbol{\theta}_i}\dot{\boldsymbol{\theta}}_i-m_{ij}\mathbf{g}^T{}^E_B\mathbf{R}\frac{\partial\mathbf{s}_{ij}}{\partial\boldsymbol{\theta}_i}\right] \tag{A3}$$

The matrix $\mathbf{A}_\phi$ is a kind of transformation matrix from the time-derivative of Byrant angle $\dot{\boldsymbol{\phi}}_B$ to the angular velocity of the trunk body $\boldsymbol{\omega}'_B$ expressed in {B} as

$$\boldsymbol{\omega}'_B=\mathbf{A}_\phi\dot{\boldsymbol{\phi}}_B$$

$$\mathbf{A}_\phi=\begin{bmatrix} cos\,\phi_{By}\,cos\phi_{Bz} & sin\phi_{Bz} & 0 \\ -cos\phi_{By}\,sin\phi_{Bz}\,cos\phi_{Bz} & 0 \\ sin\phi_{Bz} & 0 & 1 \end{bmatrix} \tag{A4}$$

Bryant angles are adopted for the rotational motion of the trunk body is $\boldsymbol{\phi}_B=(\phi_{Bx}\ \phi_{By}\ \phi_{Bz})^T$ representing the roll, pitch, and yaw angles of the trunk. The vector $\mathbf{s}_{ij}$ is the position vector of the CG point of link j in leg i in {B}, thus the relationship between $\mathbf{s}_{ij}$ and $\mathbf{r}_{ij}$ appeared in Equation (2) is $\mathbf{r}_{ij}={}^E_B\mathbf{R}\mathbf{s}_{ij}$. The matrix $\tilde{\mathbf{s}}_{ij}$ denotes the dual matrix of the vector $\mathbf{s}_{ij}$. The matrix ${}^E_B\mathbf{R}$ is the transformation matrix from {B} and {E} which is written in terms of the Bryant angles as

$${}^E_B\mathbf{R}=\begin{bmatrix} cos\phi_{By}cos\phi_{Bz} & -cos\phi_{By}sin\phi_{Bz} & sin\phi_{By} \\ cos\phi_{Bx}sin\phi_{Bz} & cos\phi_{Bx}cos\phi_{Bz} & -sin\phi_{Bx}cos\phi_{By} \\ \quad +sin\phi_{Bx}sin\phi_{By}cos\phi_{Bz} & -sin\phi_{Bx}sin\phi_{By}sin\phi_{Bz} & \\ sin\phi_{Bx}sin\phi_{Bz} & sin\phi_{Bx}cos\phi_{Bz} & cos\phi_{Bx}cos\phi_{By} \\ \quad -cos\phi_{Bx}sin\phi_{By}cos\phi_{Bz} & +cos\phi_{Bx}sin\phi_{By}sin\phi_{Bz} & \end{bmatrix} \tag{A5}$$

The matrices $\mathbf{Q}_{ij}$ and $\mathbf{R}_{ij}$ are defined to describe $\boldsymbol{\omega}'_{ij}$ which is the angular velocity of the link j in leg i as follows:

$$\mathbf{Q}_{ij}={}^B_{ij}\mathbf{R}^T\mathbf{A}_\phi$$

$$\mathbf{R}_{i1}=\mathbf{C}_1$$

$$\mathbf{R}_{i2}={}^{i1}_{i2}\mathbf{R}^T\mathbf{C}_1+\mathbf{C}_2$$

$$\mathbf{R}_{i3}={}^{i1}_{i3}\mathbf{R}^T\mathbf{C}_1+{}^{i2}_{i3}\mathbf{R}^T\mathbf{C}_2+\mathbf{C}_3 \tag{A6}$$

where ${}^{i1}_{i2}\mathbf{R}$ implies the transformation matrix from the body fixed coordinate of the link 2 to that of the link 1 both in leg i. The matrix $\mathbf{C}_k$ (k=1,2,3) are the constant coordinating matrices for the k-th joint in a leg. The joint arrangement has x-y-y rotation sequentially from the top as shown in Figure 1. In this case, the matrices $\mathbf{C}_1$, $\mathbf{C}_2$ and $\mathbf{C}_3$ are defined as

$$\mathbf{C}_1=\begin{bmatrix}1&0&0\\0&0&0\\0&0&0\end{bmatrix},\ \mathbf{C}_2=\begin{bmatrix}0&0&0\\0&1&0\\0&0&0\end{bmatrix},\ \mathbf{C}_3=\begin{bmatrix}0&0&0\\0&0&1\\0&0&0\end{bmatrix} \tag{A7}$$

Introducing these coordinating matrices, it is possible to use the relative joint coordinates. The angular velocity of link j in leg i, $\boldsymbol{\omega}'_{ij}$ can be obtained as

$$\boldsymbol{\omega}'_{ij}=\mathbf{Q}_{ij}\dot{\boldsymbol{\phi}}_B+\mathbf{R}_{ij}\dot{\boldsymbol{\theta}}_i \tag{A8}$$

Note that the body fixed coordinate of link j in leg i is located at the CG of the link with the initial orientation identical to that of {B}. The matrix $\mathbf{J}_{ij}$ is the Jacobian matrices obtained from the following relation,

$$\mathbf{J}_{ij}=\frac{\partial\mathbf{s}_{ij}}{\partial\boldsymbol{\theta}_i} \tag{A9}$$

https://doi.org/10.1017/S0263574799001058 Published online by Cambridge University Press